Oxygen states in La- and Rh-doped Sr 2 IrO 4 probed by angle-resolved photoemission and O K edge RIXS

V. Ilakovac, A. Louat, A. Nicolaou, J.-P. Rueff, Yves Joly, V. Brouet

Oxygen states in La and Rh doped Sr_2IrO_4 probed by ARPES and O K edge RIXS

V. Ilakovac,[1,2] A. Louat,[3] A. Nicolaou,[4] J.-P. Rueff,[4,1] Y. Joly,[5] and V. Brouet[3]

[1] *Sorbonne Université, CNRS, Laboratoire de Chimie Physique – Matière et Rayonnement, F-75252 Paris, France**

[2] *Département de Physique, Université de Cergy-Pontoise, F-95031 Cergy-Pontoise, France*

[3] *Laboratoire de Physique de Solides, CNRS UMR 8502, Univ. Paris Sud, Université Paris Saclay, Orsay, France*†

[4] *Synchrotron SOLEIL, L'Orme des Merisiers, Saint-Aubin, B.P. 48, F-91192 Gif-sur-Yvette, France*‡

[5] *Univ. Grenoble Alpes, CNRS, Grenoble INP, Institut Néel, 38000 Grenoble, France*§

(Dated: December 21, 2018)

Iridates are often viewed as an equivalent of cuprates with strong spin-orbit coupling. As such, they offer a new way to study the physics of Mott insulators. The hybridization with oxygen is of course essential in both compounds and may play a crucial role in the doping process. It could be quite different in the two families, iridates being $5d$ transition metals with different orbital geometries. But this difference has not been studied in details so far. We present a combined ARPES and O K-edge study to document this aspect in Sr_2IrO_4, pure and doped with 4% La and 15% Rh. We evidence different charge transfer excitations and distinguish those associated with apical or in-plane oxygens. We observe a specific evolution of one excitation upon Rh doping, which suggests a more itinerant nature of the holes related to the apical oxygen. This gives information on the way doping proceeds in iridates.

I. INTRODUCTION

Sr_2IrO_4 is attracting strong interest due to its large spin-orbit coupling, uncommon in the context of strongly correlated oxides. This strong SOC creates a situation with a half-filled band at the Fermi level, which is analogous to cuprates[1]. Indeed, both systems have an insulating and antiferromagnetic ground state[2]. The question on whether superconductivity could be obtained upon doping iridates has emerged[3,4], although it has not been realized in bulk compounds up to now.

Despite the analogous situation of a half-filled band, there remains many differences, because the orbitals involved are quite different. In particular, this could give a different role to the oxygen ligand. In cuprates, the half-filled band has $d_{x^2-y^2}$ symmetry. In iridates, this role is fulfilled by the J_{eff}=1/2 band, with equal weight of the d_{xz}, d_{yz} and d_{xy} orbitals, which do not point directly to the in-plane oxygens. On one hand, a weaker hybridization with oxygen is expected for t_{2g} orbitals compared to e_g; on the other hand, a larger one is expected for $5d$ transition metals. Moreover, contrary to the $d_{x^2-y^2}$ orbitals, the J_{eff}=1/2 orbitals have strong out-of-plane component, and may couple more strongly to the apical oxygen of the oxygen octahedra surrounding the Ir atom. Finally, it is well known that cuprates are charge transfer compounds, their charge transfer energy Δ of 2-3 eV being smaller than the Mott gap (5 eV). Consequently, doped holes mainly reside in the four in-plane oxygens surrounding Cu and couple antiferromagnetically to it to form a Zhang-Rice singlet[5]. This could be different in iridates, where the Mott gap of about 0.6 eV is probably smaller than the charge transfer excitations[6].

There have not been many experiments specifically testing the coupling with oxygen in iridates, beyond XAS studies[7]. We propose here a coupled ARPES and RIXS study, complemented by DFT calculations, to discuss this point. There have been many ARPES studies of Sr_2IrO_4, undoped[1] and doped[8–10], but they focused on the Ir states near the Fermi level. Similarly, previous RIXS studies, both at the Ir L edge[11–13] and O K edge[14,15], focused on the low energy excitations.

With ARPES, we observe directly the oxygen valence bands and find a good agreement with the calculation, rigidly shifted by -0.55 eV, validating the use of density of states obtained from such calculations. With RIXS, we distinguish the contribution of apical and in-plane oxygens, by tuning the incoming photon energy to their different excitation thresholds. We reproduce the RIXS spectra with a simple computation based on a convolution of a product of occupied and unoccupied density of states with the resonant lorentzian. We then focus on the fluorescent or Raman nature of these excitations, which gives information on the lifetime of the intermediate state of the RIXS process[11,16]. This lifetime will typically be longer for a localized state (giving Raman behavior) and shorter for a metallic state (giving fluorescent decay). We find that at least one charge transfer excitation evolves from Raman to fluorescent behavior, as a function of the photon excitation energy.

We then study the evolution of the RIXS spectra when doping with La or Rh, which are two alternative ways to get closer to the metallic state[8,17], inducing respectively electron[9] and hole dopings[18]. We observe a large fluorescence in the case of Rh that seems to be specific to the apical site. Our study suggests a rather strong discrepancy between the hole and the electron doping, characterized by different couplings to oxygen, which was quite unexpected. This information on the behavior of the introduced carriers could be crucial to better understand the role of oxygen in the doping process.

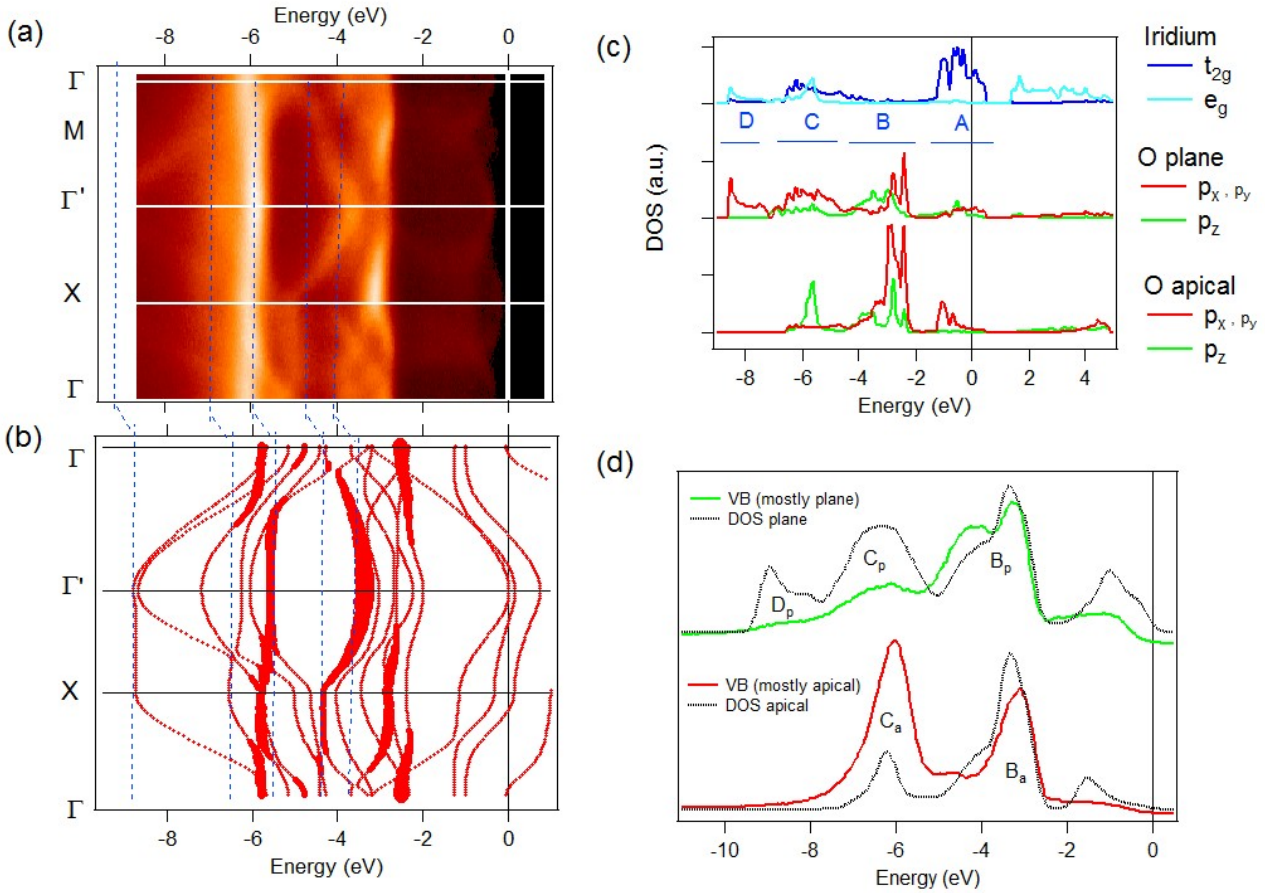

Figure 1. (a) Energy-momentum plot of the ARPES intensity obtained in Sr_2IrO_4 at 100 eV photon energy along a path ΓMΓ'XΓ. (b) Band calculation for Sr_2IrO_4 including spin-orbit coupling but neglecting the rotation of oxygen octahedra. The weight of the apical p_z oxygen orbital is represented as marker size. Blue dotted lines underline the correspondence between measured and calculated features, after a shift of 0.55 eV. (c) Density of states calculated for Sr_2IrO_4 including oxygen octahedra rotations. Partial weights are shown, as indicated. (d) Integrated valence bands (VB) measured by ARPES in experimental configurations favoring apical (red, top) or in-plane (green, bottom) oxygens. Calcualted DOS in (c) convoluted by a Gaussian for apical (top) and in-plane (bottom) oxygens. Indexes a/p of the structures A, B, C, D, are for apical/in-plane. The energy scales are shifted between spectra (bottom) and calculation (top) by 0.55eV.

II. EXPERIMENTAL AND CALCULATION DETAILS

The samples were prepared using a self-flux method as reported in[8]. ARPES experiments were carried out at the CASSIOPEE beamline of SOLEIL synchrotron, with a SCIENTA R-4000 analyser and an overall resolution better than 15 meV. All data shown here were acquired at a photon energy of 100 eV and at a temperature of 50 K. O K edge (≈ 530 eV) RIXS data were acquired at the SEXTANTS beamline[20] of the synchrotron SOLEIL by means of the AERHA spectrometer[19] with an overall energy resolution of 130 meV. The scattering angle was fixed and the incoming light polarization was horizontal (π polarization). X-ray Absorption Spectroscopy (XAS) measurements were performed in the total electron yield mode with the beamline resolution set to 110 meV. RIXS measurements were performed at 25 K. XAS calculation were performed with the FDMNES code[21,22], using the full potential, relativistic, approach, including SOC and a Hubbard correction of U = 2 eV at the iridium site, while the core-hole screening effect was minimized. In order to calculate the RIXS spectra, the site and orbital projected density of states were calculated by Wien2k program[23] using the coordinates of the $I4_1/acd$ space group structure measured by Crawford et al.[24].

III. RESULTS AND DISCUSSION

A. ARPES in pure Sr_2IrO_4

In Fig.1a, the electronic structure measured by ARPES in Sr_2IrO_4 is displayed on a large energy window. Weak Ir t_{2g} states are observed between 0 and -2 eV binding energies, as already discussed in details in the literature[1,8,9].

At higher binding energies, between -3 and -9 eV, many well defined and dispersing bands are observed. Comparison with Fig.1b shows that they correspond well to the oxygen bands expected from an ab-initio calculation. For more clear comparison, we use here a calculation in a simplified structure, neglecting the rotation of the oxygen octahedra. This calculation gives a very similar density of states compared to that using the full structure, shown in Fig.1c and used later for the analysis of RIXS.

In our measurement, there is a predominance of the p_z orbital of the apical oxygen, which has a very strong cross section for ARPES (as it is out of plane) and is in the top cleaving plane. Indeed, we show with fat bands the weight of oxygen apical p_z in Fig.1b and this underlines nearly all dominant features in the measurement: a very strong non-dispersing band at -6 eV, a band dispersing from -4 to -5.8 eV and the top of the bands near -3 eV. As indicated by blue dotted lines, these features overlap well with our measurements, but they have to be shifted down by 0.55 eV. This value is nearly that of the gap opening in the J_{eff}=1/2 band. However, it is not clear whether the oxygen bands should move together with the band gap. Alternatively, a recent GW calculation predicted a 0.5 eV shift of oxygen states relative to the Ir states[25].

The density of states presented in Fig.1c helps to identify the origin of these bands. We can distinguish four different regions labelled A, B, C, D on the graph. The A region corresponds to the partially filled t_{2g} Ir orbitals, hybridizing with oxygen, B to non-bonding oxygen orbitals, C to bonding oxygen orbitals of mainly t_{2g} character (with the exception of the non-dispersing band at -6 eV, which results from hybridization of Ir d_{z^2} and oxygen apical p_z) and D to bonding oxygen orbitals of mainly $d_{x^2-y^2}$ character. The e_g bands are essentially empty extending between 1 and 5 eV above E_F. In the unoccupied part, the gap between t_{2g} and e_g is 0.8 eV.

To clarify the agreement, we present in Fig.1d integrated ARPES spectra where the dominant contribution comes from the apical oxygen (red, bottom spectra) or the in-plane oxygen (green, top spectra) site. These are tuned by the angle of incidence of light on the sample surface. We compare them with the corresponding calculation of the DOS, broadened by a convolution with a gaussian of 0.2 eV linewidth, and shifted for 0.55 eV, taking into account the gap. The qualitative shape is well described, the peaks are broader for the in-plane oxygen with a third peak D_p absent at the apical site. The shift of the calculated scale brings the main features in good coincidence, especially the first edge of the valence band at -2.8 eV both for in-plane and apical sites. We note that the shift might be slightly reduced for the strong feature B_a, as it occurs at 0.2 eV higher binding energy compared to the the experimental peak. The other features are too broad to discuss the possibility of such a shift.

We have obtained similar results in La and Rh doped Sr_2IrO_4, ruling out a strong change of the structure of the occupied oxygen bands with doping. This comparison validates the use of ab-initio calculations to analyze other measurements, such as the RIXS data we will now present to get complementary information of the role of oxygen.

B. O K-edge RIXS in pure Sr_2IrO_4

O K edge XAS spectra are presented in Fig.2a. The incident light wave vector was either normal to the sample surface (NI, red dots) or in grazing incidence (GI, black dots), at 20° relative to the sample surface. The spectra are normalized to the same value far from the edge (580 eV). Its polarization was in the horizontal plane (see inset). Consequently, mainly p_x/p_y oxygen orbitals are excited in NI and p_z in GI, which involves in turn Ir orbitals according to their interaction. Lower part of Fig.2a shows calculated O K edge XAS spectra and their apical/in-plane site decomposition. The unoccupied Ir $5d$ states are shown in Fig.2b and their orientation relative to the O $2p$ orbitals is sketched in Fig.3: Ir d_{xz}/d_{yz} hybridizes with the in-plane p_z and the apical p_x/p_y, while d_{xy} couples mainly to the in-plane p_x/p_y. Higher energy e_g orbitals and $d_{z^2}/d_{x^2-y^2}$, point to the apical p_z and the in-plane p_x/p_y, respectively.

According to the XAS calculation, the first two peaks, at $h\nu = 528.80$ eV and $h\nu = 529.5$ eV, correspond mainly to the in-plane oxygen, but the contribution of the apical oxygen to the first peak is relevant in the NI spectra. Previous works[1,7] attribute the first peak exclusively to the apical site, on the basis of the core-level shift, due to the difference in the apical/in-plane environments. Effectively, our calculation confirms that the core-level shift of the in-plane site is 0.29 eV higher compared to the apical site, which is more evident in the GI ($\theta = 0°$) calculated spectra. Despite this difference, the DFT calculation of these unoccupied states underestimate the apical character of the first XAS peak, as will be demonstrated by RIXS measurements in the following.

The first peak is clearly visible in the NI spectra, meaning that it is mainly the result of d_{xz}/d_{yz} - p_x/p_y hybridization. The second peak is 2-3 times stronger for the GI compared to the NI. It thus selects d_{xz}/d_{yz} hybridized with the in-plane p_z much more than the d_{xy} coupled either with the in-plane or the apical p_x/p_y. At higher photon energy, the large feature/shoulder from about $h\nu = 531$ eV corresponds to the transition to the O $2p$ states hybridized with Ir e_g states. The prominent peak at 531 eV is from apical oxygen $2p_z$ coupled to $5d_{z^2}$.

O K edge RIXS spectra are presented in Fig.4 in two ways, in the energy-loss scale (E_L), and in the emitted energy scale, see Fig.4b,c, respectively. Features with Raman character are easily identified in the energy-loss scale, as their position does not change when the incident energy is altered, while structures with strictly fluorescent behavior do not shift in the emitted-energy scale. The Raman/fluorescent character of an excitation measures the rate of incoherent scattering of the pho-

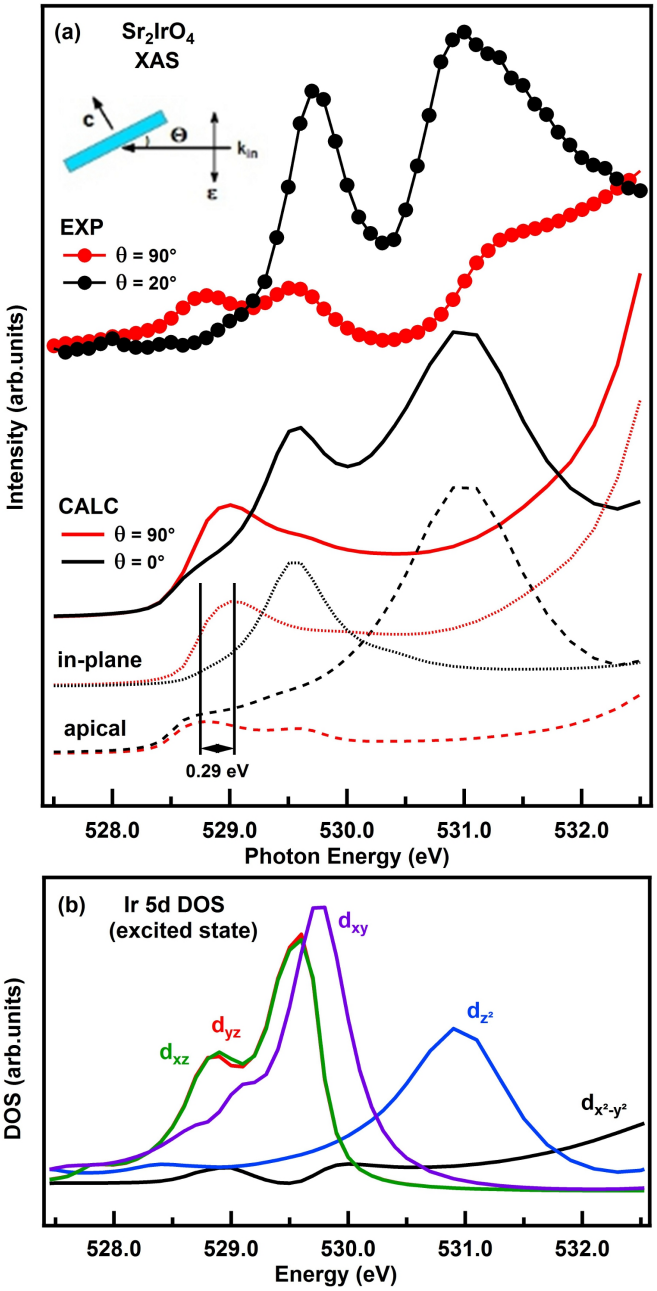

Figure 2. (a) Polarization dependence of the measured (dots) and calculated (lines) O K edge XAS spectra. Inset presents the experimental geometry. Doted lines are corresponding contributions of the apical and the in-plane oxygen sites. (b) DOS of the unoccupied Ir 5*d* states, hybridizing with O 2*p* states, for the case when the apical oxygen site is excited.

toexcited electron in the intermediate state of the RIXS process (the final state of the absorption process)[11]. If the photoexcited electron is promoted to a state where the information on its phase is conserved for a time of the order of the lifetime of the intermediate state, the absorption and emission processes will occur coherently, and the excitation will have Raman character. On the

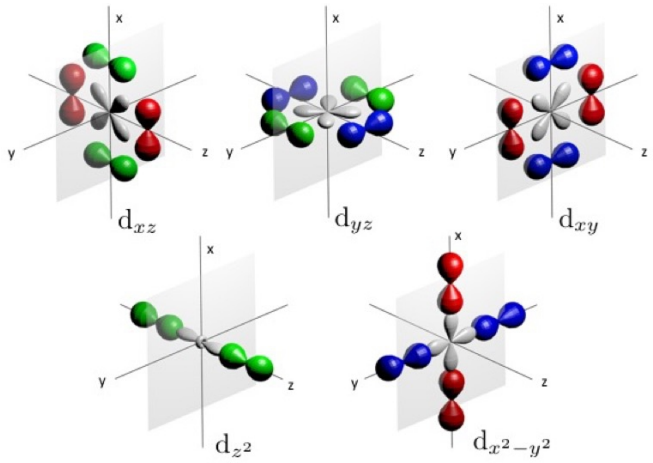

Figure 3. Sketch of the relative positions of O 2*p* and Ir 5*d* orbitals. Gray lobes in upper/lower panels present Ir 5*d* t_{2g}/e_g orbitals. Red/blue/green lobes are for O $p_x/p_y/p_z$ orbitals hybridized with corresponding Ir states. Light gray square indicates the xy plane, including Ir and in-plane oxygens.

other hand, when the photoexcited electron is accommodated to a state where the information of its phase is quickly lost, the absorption and emission processes will be decoupled, and the feature in the RIXS spectra will have fluorescent behavior.

Previous studies have mainly focused on the low energy Raman structures, visible both in Ir $L_{3/2}$ edge RIXS spectra[12,13] and O K edge RIXS spectra[14,15]. These are spin-orbit exciton (feature labelled E at 0.65 eV energy loss in the Fig.4b) and single- and bi-magnon excitations at about 100 meV, and 150 meV, respectively, visible in our data as a shoulder near the elastic peak. We focus here on the features at larger energy loss. The overall shape of the O K edge RIXS spectra strongly changes with the incoming photon energy, particularly in the $h\nu$ = 528.8-530.0 eV range. At the excitation energy of the first peak, two rather sharp peaks are distinguished, which can be related to the B_a and C_a structures in the DOS (see Fig.1c and Fig.4c). When the incoming light is tuned to the second peak, corresponding mainly to the in-plane oxygen, besides two structures B_p and C_p, another large feature D_p appears (see Fig.1c and Fig.4b). From the RIXS data we can now conclude that the first peak is much more related to the excitation of the apical site than predicted by the XAS calculation.

As the RIXS spectra correspond quite well to the occupied DOS in Fig.1, we attempt a description by a product of occupied and unoccupied site-projected density of states, convoluted by the resonant lorentzian:[26,27]

$$F(\Omega,\omega) = \int_{\epsilon} d\epsilon \frac{\rho(\epsilon)\rho'(\epsilon+\Omega-\omega)}{(\epsilon-\omega)^2+\frac{\Gamma^2}{4}} \qquad (1)$$

ρ and ρ' are here densities of occupied and unoccupied oxygen 2*p* states, Ω and ω are the incoming and outgoing

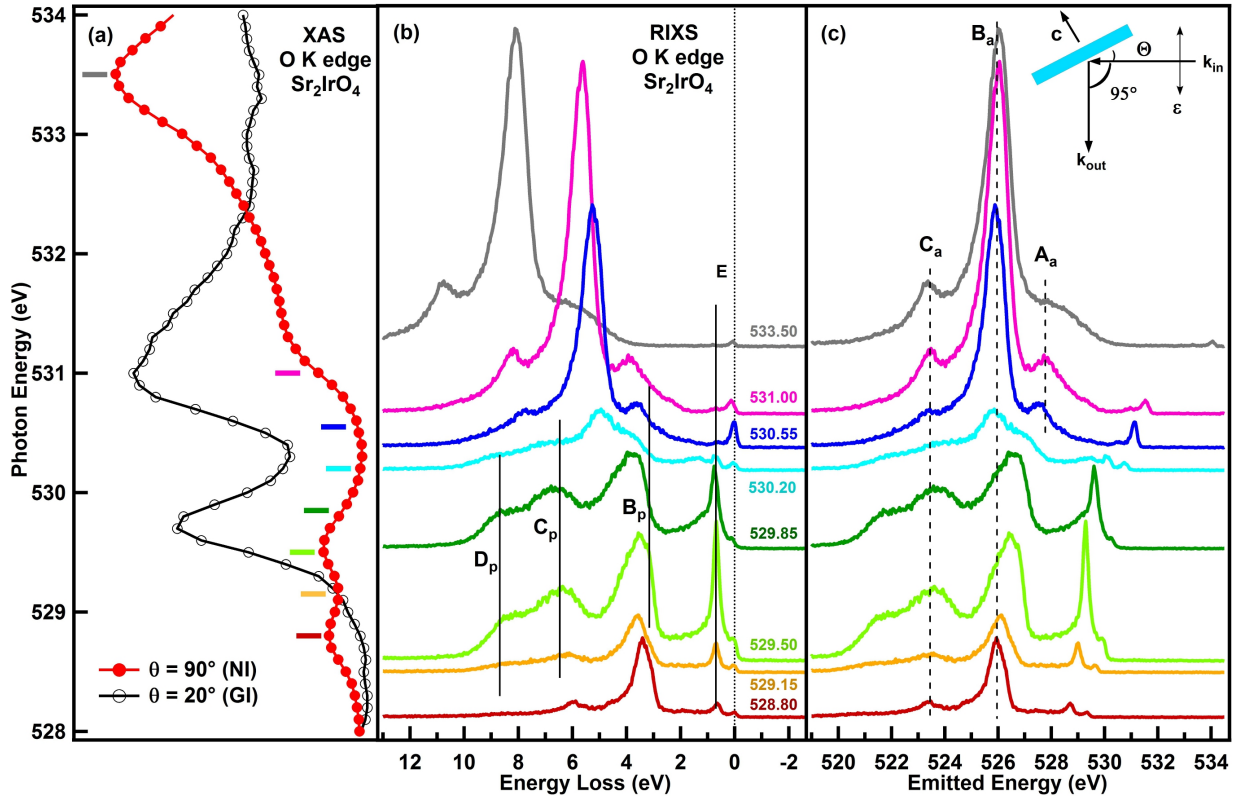

Figure 4. O K edge XAS (a) and RIXS (b, c) spectra of Sr_2IrO_4. RIXS spectra, collected at photon incidence of $\theta = 45°$, are presented in the energy loss, E_L (b) and emitted energy scale (c). Incident photon energies are indicated on the XAS spectrum by the line of the same color. Experimental geometry showing the incoming wave vector (k_{in}), outgoing wave vector (k_{out}), the direction of the incoming photon polarization (ε) related to the surface of the sample and its crystal axis c, is shown in the inset of (c).

photon energies, respectively, and Γ corresponds to the core-hole lifetime broadening. The calculation procedure is illustrated in Fig.5.

This simple approach assumes that each empty state is connected with each occupied state with the same matrix element. This approximation is not correct in the case of strong variations in the matrix elements related to the excitonic nature of the intermediate state and thus cannot describe well metal L edge RIXS of 3d compounds. It is however quite correct for the oxygen K edge even if it does not include any final-state-interference effects and thus it can not evaluate correctly the RIXS cross section. In particular, the region $E_L < 2$ eV, where the spin-orbit exciton (E in Fig.4b), single- and bi-magnons are observed is not correctly described. Moreover, the gap of Sr_2IrO_4 of about 0.5 eV is not included in the calculation. For the peaks at $E_L > 2$ eV, one can expect a better agreement. Our calculation describes well fluorescence-like excitations, which shift in the E_L scale. However, at the oxygen K edge, one can expect charge transfer (CT) excitation resulting of an annihilation of an oxygen $2p$ hole (strongly hybridized with a metal d orbital) by a photoexcited O 1s electron, followed by the decay of a different O $2p$ electron, filling the O $1s$ core hole and

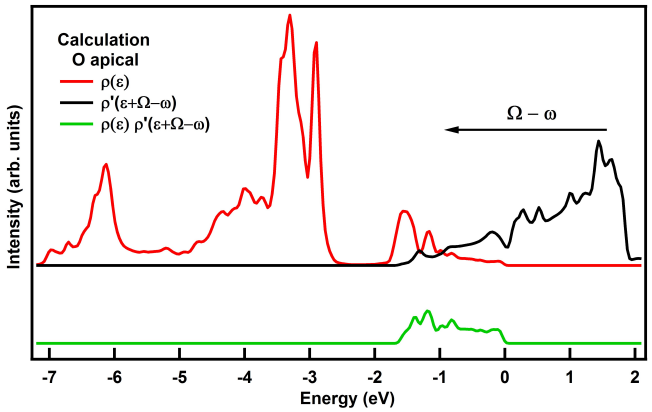

Figure 5. Illustraion of the RIXS calculation procedure taking the O apical DOS as example. For each energy loss $E_L = \Omega - \omega$, the occupied DOS is multiplied by the unoccupied DOS shifted for $(\Omega - \omega)$, and the product is then convoluted by the resonant lorentzian.

leaving the system in an excited state[16]. CT excitations have likely similar spectral form as the fluorescence, but

are sometimes distinguished by their Raman behavior. Our calculation should therefore give good guidance to identify the origin of the peaks at $E_L > 2$ eV.

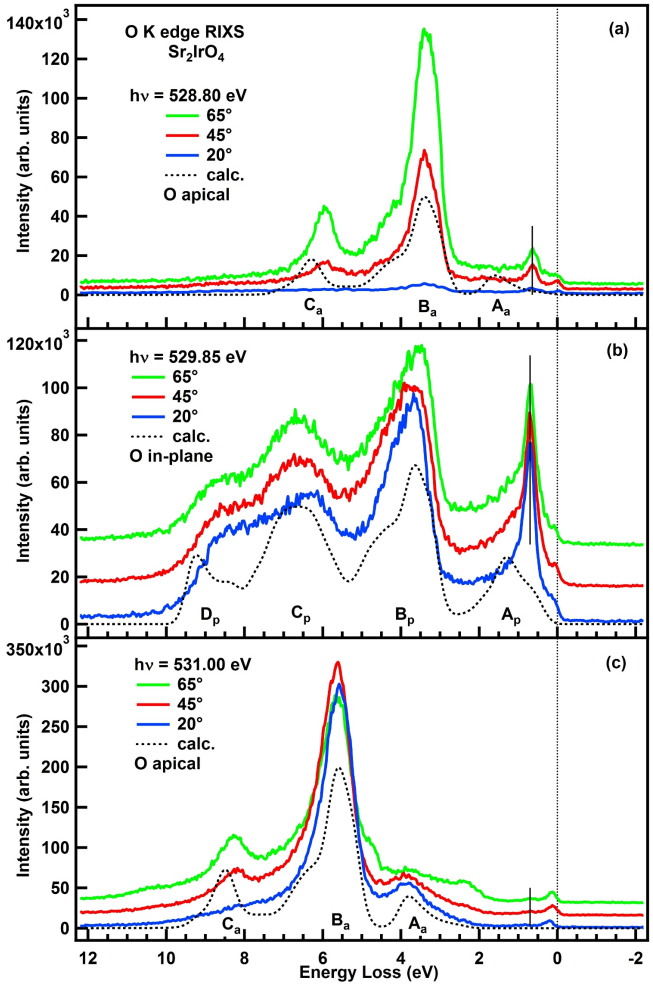

Figure 6. Incident angle dependent O K edge RIXS spectra of Sr_2IrO_4 for $h\nu = 528.80$ eV (a), 529.85 eV (b), 531.00 eV (c). The (grazing) incidence angle was set to $\theta = 20°$, 45° and 60°. The vertical solid line indicates the position of the spin-orbit exciton. The calculated spectra should be compared to the experiment performed at $\theta = 45°$. The B_a/B_p is aligned with the most prominent peak in the experimental spectra.

In Fig.6, we compare experimental spectra measured under different polarization conditions for three selected photon energies with the calculation including the contribution from the oxygen dominating the XAS at this photon energy. This is the apical oxygen for $h\nu = 528.8$ eV (a) and 531 eV (c) and the in-plane oxygen for $h\nu = 529.85$ eV (b). There is a good overall correspondence and, in particular, this explains well the appearance of the D_p feature in (b) and the alternation between sharp and broad features, corresponding to apical and in-plane. This comparison confirms that the contribution of the

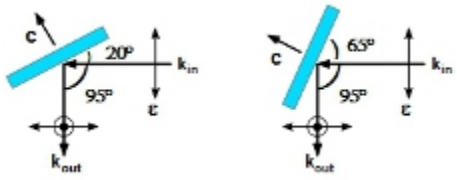

Figure 7. For the detector position at a scattering angle which is almost equal to 90°, the absorption to the unoccupied p_z states is enhanced [$\theta = 20°$] (suppressed [$\theta = 65°$)]), while the intensity of the light emitted from the occupied p_z states is decreased (enhanced). For the p_x/p_y states, the polarization dependence is opposite but less strong, as one of emitted components is perpendicular to the (k_{in},k_{out}) plane and is always detected.

apical and the in-plane oxygen can be disentangled from the RIXS spectra, a conclusion already reached in[15].

Spectra at different incident angles (θ, see Fig.7) allow to probe the nature of the states involved in the photoabsorption and the emission process. The angular (θ) dependence at $h\nu = 528.8$ eV (Fig.6a) is particularly strong. For ε almost parallel to the crystal axis c ($\theta = 20°$, GI), its intensity vanishes, while for ε almost perpendicular to c ($\theta = 65°$), the intensity of all the features is strongly enhanced. This is similar to the XAS behavior and originates from the poor hybridization of Ir t_{2g} and apical oxygen $2p_z$ states, strongly suppressing this absorption channel.

The angular (θ) dependence is smaller at $h\nu = 529.85$ eV (Fig.6b) as it is connected to the in-plane oxygen, which has more equal contributions from p_x/p_y and p_z. We have chosen this incident energy as our normalization reference because the spectra do not change considerably when θ is varied, at least in the region of the high energy loss we are interested in: the spectra at different incident energies are multiplied by a factor that yields the same integral intensity as the $h\nu = 529.85$ eV spectra of the three incident angles. Similar way of normalization was applied in the previous O K edge study of Sr_2IrO_4[15].

The polarization dependence of the $h\nu = 531$ eV spectra (Fig.6c), dominated again by the apical oxygen, is still strong, but completely different from that of the $h\nu = 528.8$ eV spectra. At this photon energy, there is a significant absorption for θ=20° because of the contribution of d_z^2, which is strongly hybridized with apical p_z. The intensity of the strong peak B_a at $E_L = 5.5$ eV is almost constant, but the side peaks A_a and C_a have opposite evolution with θ. The intensity for peak A_a at $E_L = 4$ eV is largest for $\theta = 20°$, while that for peak C_a at $E_L = 8$ eV is largest for $\theta = 65°$. This angular dependence can not be explained exclusively by the photoabsorption process but the detector position relative to the axes of the single crystal has to be taken into account. Indeed, the apical oxygen DOS (see Fig.1) has a p_x/p_y related structure at low energy (A_a) and a p_z feature at high energy (C_a).

For the detector position at 95° relative to the incoming light, the emission from the p_z states is enhanced for $\theta = 65°$, while this from the p_x/p_y is enhanced for $\theta = 20°$. The agreement of the polarization dependence with the orbital content predicted by the calculation validates this analysis.

In our calculation, all three structures are reproduced by the same procedure, which underestimates *dd* excitations. In a previous work, $E_L = 3.5$ eV (our B_p feature) was attributed to the equivalent of the *dd* ($t_{2g} \rightarrow e_g$) excitation, while the two large structures in the range of $E_L > 6$ eV are attributed to the charge-transfer (CT) excitation.[15] Nevertheless, at the Ir edge[11], there is a peak centered at 3.2 eV, which is attributed to a CT excitation. The B_p feature is the most pronounced feature in our O K edge RIXS spectra. While we cannot exclude that *dd* excitations contribute to this peak, we would rather expect a small *dd* cross section at the excitation energy corresponding to O $2p$ - Ir t_{2g} hybridized states. Moreover, there is a clear evolution of the lineshape as a function of photon energy from a sharp peak to broad to sharp again, which is well described by the change of the DOS from apical to plane and is not expected for a *dd* excitation. Note that a similar evolution is observed for the C_p peak.

We now discuss the Raman/fluorescent behavior of the different features in our RIXS spectra. The fluorescent nature of the features observed at photon energies higher than $h\nu = 530.5$ eV is clear. For lower energies, and for $E_L > 2$ eV, there are several components which are not resolved in the spectra, resulting in structures which are broad compared to the change of the excitation energy. Therefore their Raman/fluorescence behavior is not straightforward to decide.

At $h\nu > 530.5$ eV, sharp A_a, B_a, C_a peaks have obviously fluorescent behavior (see Fig.4c). The energy separation of structures B_a and C_a is slightly smaller (0.4 eV) than the calculated value. We noticed that the B_a/C_a separation is slightly (0.2 eV) reduced in ARPES, but this separation is enlarged in RIXS. This may mean that one of the peaks has not fully reached the florescence regime. The calculated structure A_a is not observed in the $h\nu = 528.80$ eV spectra (see Fig.4a). Its cross section should indeed be decreased, when the low-energy excitations, like spin-orbit exciton, single- and bi-magnons, involving O $2p$ states hybridized with Ir t_{2g} states, are prefered RIXS channels.

The peak E is the only feature showing obvious Raman behavior (see Fig.4b) in the whole excitation energy range. We note that it disappears for photon energies corresponding to excitations above t_{2g} states. For the three large structures B_p, C_p, D_p and the E-peak shoulder A_p, which are quite broad and appear in a small excitation energy range of the in-plane oxygen, it is less clear. 2D map in previous O K edge RIXS measurements with the grazing incident π polarized (ε almost parallel c) in the range of $h\nu = 529.4$–529.9 eV, suggests that $E_L = 3.5$, 6.5 and 8.8 eV have Raman character.[15] We agree that the edge of B_p in Fig.4 is better described by a Raman mode up to 529.85eV. Although it changes from apical to in-plane over this photon energy range, our ARPES spectra have shown that both DOS (apical and in-plane) have a similar edge so that this should not produce a shift. But, at 530.2 eV, there is clearly a double peak structure, that seems to originate from the apical contribution in fluorescence regime and the in-plane contribution still in Raman regime. This observation will acquire more significance as we turn to the doping dependence.

C. La- and Rh-doped Sr_2IrO_4

O K edge XAS spectra of pure, 15% Rh-, and 4% La-doped Sr_2IrO_4 are shown in Fig.8, for two incident angles $\theta = 90°$ (NI) and 20° (GI). Rh-doping induces holes[10,18,28], while La dopes with electrons[8,9]. These two different ways of doping move both compounds close to a metallic state[8].

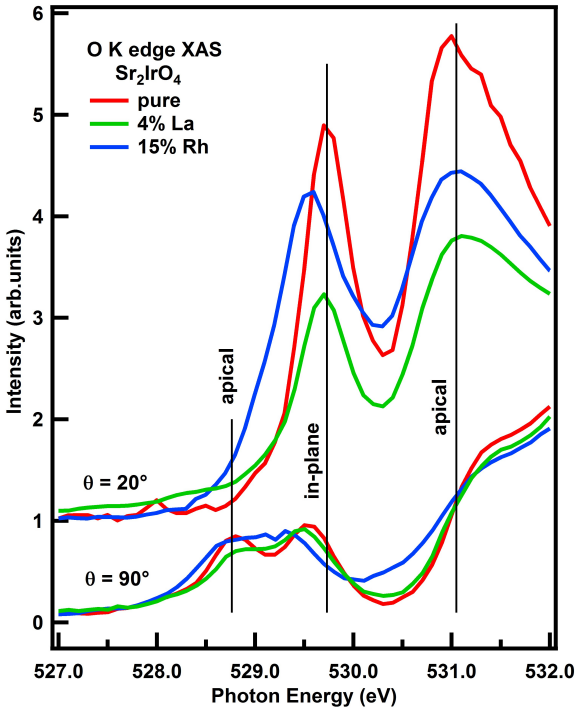

Figure 8. XAS spectra of pure, 4% La-doped and 15% Rh-doped Sr_2IrO_4, for two incident angles, NI ($\theta = 90°$) and GI ($\theta = 20°$).

For Normal Incidence ($\theta = 90°$), the double pre-peak structure, corresponding to apical and in-plane oxygens, is clearly resolved in the pure and La doped spectra, but less clearly in the Rh doped case. This might be due to a low energy shift of the in-plane p_x/p_y states for about 0.3 eV, induced by Ir/Rh substitution, while

the apical p_x/p_y states are less affected. A similar effect was observed for pure Sr_2RhO_4[7] and as a function of Rh doping[29]. This indicates a modification of the electronic environment of both oxygen sites, probably related to the weakening of the in-plane O $2p$ - Ir t_{2g} hybridization.

At the same time, for GI ($\theta = 20°$), the strong feature at $h\nu = 528.85$ eV is quite similar in the pure- and the La-doped-sample spectra. Conversely, for the Rh-doped-sample, it is shifted to the lower energy, similarly to the NI peak, and enlarged on the low energy side. This might be due to the Rh-doping related accommodation of holes on apical oxygen sites and/or a distribution of values of the apical-plane splitting.

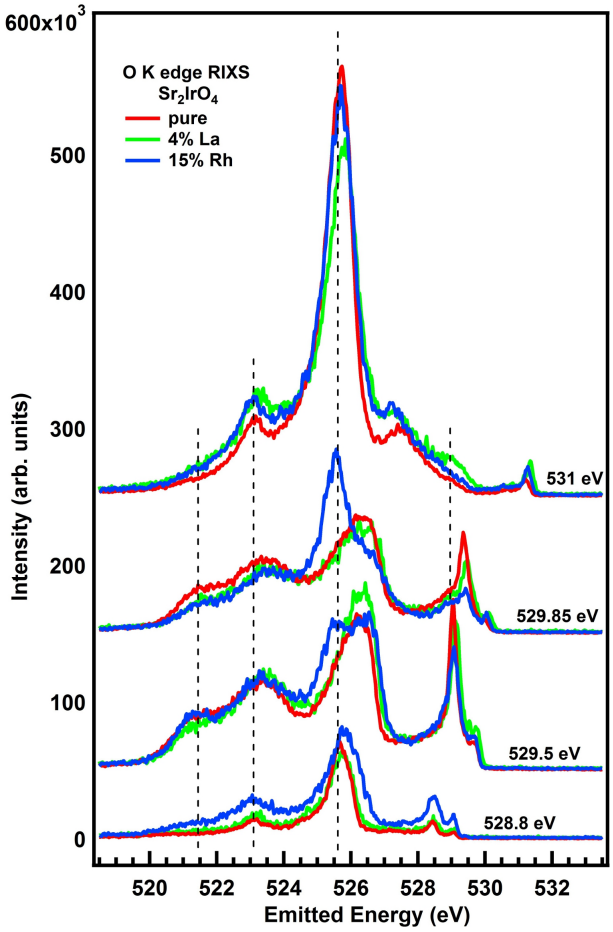

Figure 9. Selected O K edge RIXS spectra of pure, 4% La- and 15% Rh-doped Sr_2IrO_4 presented in the energy loss (a) and emitted energy (b) scale, collected at $\theta = 45°$. Vertical solid lines in the energy loss scale indicate features with Raman behavior, while dotted lines in the emitted energy scale points to features which behave as fluorescence and are related to the DOS structures.

O K edge RIXS spectra of the three samples are shown in Fig.9, in the emitted energy scale. In order to compare the spectra, we adopted the same normalization scheme as for the pure system: the spectra at different excitation energies are multiplied by a factor that yields the same integral intensity as the $h\nu = 529.85$ eV spectra of the three compounds. Regarding excitations at less than $E_L = 1$ eV, for the three systems their intensity is highest in the $h\nu = 529.5$ eV spectra, even if it seems to resonate at slightly lower energy in the Rh-doped system.

For the excitations at higher energy loss, we first remark that the spectra at high photon energies overlap well in the 3 compounds, implying there is no strong modification of the DOS itself. Regarding high energy loss structures, pure and 4% La-doped samples are quite similar. The 15% Rh-doped sample however shows differences. The fluorescent part of the B peak appears at much lower photon energy and/or with larger intensity. It also extends to lower E_L in the $h\nu = 528.80$ eV spectrum.

On one hand, one would expect fluorescence to dominate more strongly when a sample becomes more metallic, which agrees with the trend observed for Rh doping. However, the difference between La and Rh is difficult to understand, as their resistivities are relatively close[8]. More specifically, the behavior in the Rh case makes it also quite clear that the fluorescent part of B is sharp, typically like the contribution from the apical site. This suggests a different behavior for electrons coupled to the apical or the in-plane site, the former ones being more strongly delocalized. From the XAS spectra, we know that the threshold for exciting apical and in-planes oxygen sites are somewhat different for Rh. From this alone, we would only expect the in-plane contribution (i.e. large B, C and D peaks) to appear at slightly smaller photon energies, which does not explain our observation. We therefore suggest that there is a real evolution of the environment of the apical site specific to Rh, which favors delocalization of the charge carriers on this site. Conversely, electrons doped by La may bound strongly with the in-plane oxygen and delocalize less efficiently.

IV. CONCLUSION

Our study gives detailed information on the oxygen states in iridates. With ARPES, we have fully mapped their dispersion, which is found in good agreement with DFT calculations, albeit with a shift of 0.55 eV to lower binding energies, that may be explained by non-local effects[25]. Using RIXS, we show how the contribution of apical and in-plane oxygens can be decoupled using different photon energies and polarizations. Their shape is well described by a convolution of a product of occupied and unoccupied DOS with the resonant lorentzian. At least one of the features in the high-energy-loss part of the RIXS spectra evolves with photon energy from a Raman (localized-like) to a fluorescent (itinerant-like) behavior. Interestingly, we find a strong difference in the case of 15% Rh substitutions (hole doping), where electrons excited to apical oxygen (unccupied) states are found to be more itinerant. This is not the case for 4% La substitu-

tions (electron doping), although this doping provides a similar metallic state as the Rh doping in transport measurements. This suggests that the coupling with oxygen plays a different role in hole and electron doped case. Our O K edge RIXS results reveal an asymmetry between electron and hole doping, which is important to take into account for an accurate description of the electronic properties of doped iridates.

V. ACKNOWLEDGEMENT

Financial support from the French National Agency ANR-15-CE30-0009-01 SOCRATE and the Investissement d'AvenirLabEx PALM (Grant No. ANR-10-LABX-0039-PALM) is acknowledged. V.I. thanks Amélie Juhin and F. M. F. de Groot for enlightening discussions.

* vita.ilakovac-casses@upmc.fr
† alex.louat@u-psud.fr
‡ alessandro.nicolaou@synchrotron-soleil.fr
§ yves.joly@neel.cnrs.fr

[1] B. J. Kim, H. Jin, S. J. Moon, J.-Y. Kim, B.-G. Park, C. S. Leem, J. Yu, T. W. Noh, C. Kim, S.-J. Oh, J.-H. Park, V. Durairaj, G. Cao, and E. Rotenberg, Phys. Rev. Lett. **101**, 076402 (2008).
[2] M. Ge, T. F. Qi, O. B. Korneta, D. E. De Long, P. Schlottmann, W. P. Crummett, and G. Cao, Phys. Rev. B **84**, 100402 (2011).
[3] F. Wang and T. Senthil, Phys. Rev. Lett. **106**, 136402 (2011).
[4] Y. K. Kim, N. H. Sung, J. D. Denlinger, and B. J. Kim, Nat. Phys. **12**, 37 (2016)
[5] F. C. Zhang and T. M. Rice, Phys. Rev. B **37**, 3759 (1988)
[6] V. M. Katukuri, H. Stoll, J. van den Brink, and L. Hozoi, Phys. Rev. B **85**, 220402 (2012)
[7] S. J. Moon, M. W. Kim, K. W. Kim, Y. S. Lee, J.-Y. Kim, J.-H. Park, B. J. Kim, S.-J. Oh, S. Nakatsuji, Y. Maeno, I. Nagai, S. I. Ikeda, G. Cao, and T. W. Noh, Phys. Rev. B **74**, 113104 (2006).
[8] V. Brouet, J. Mansart, L. Perfetti, C. Piovera, I. Vobornik, P. Le Fevre, F. Bertran, S. C. Riggs, M. C. Shapiro, P. Giraldo-Gallo, and I. R. Fisher, Phys. Rev. B **92**, 081117 (2015).
[9] A. de la Torre, S. McKeownWalker, F. Y. Bruno, S. Ricco, Z. Wang, I. GutierrezLezama, G. Scheerer, G. Giriat, D. Jaccard, C. Berthod, T. K. Kim, M. Hoesch, E. C. Hunter, R. S. Perry, A. Tamai, and F. Baumberger, Phys. Rev. Lett. **115**, 176402 (2015).
[10] Y. Cao, Q. Wang, J. A. Waugh, T. J. Reber, H. Li, X. Zhou, S. Parham, S.-R. Park, N. C. Plumb, E. Rotenberg, A. Bostwick, J. D. Denlinger, T. Qi, M. A. Hermele, G. Cao, and D. S. Dessau, Nat. Commun. **7**, 11367 (2016).
[11] K. Ishii, I. Jarrige, M. Yoshida, K. Ikeuchi, J. Mizuki, K. Ohashi, T. Takayama, J. Matsuno, and H. Takagi, Phys. Rev. B **83**, 115121 (2011).
[12] J. Kim, D. Casa, M. H. Upton, T. Gog, Y.-J. Kim, J. F.Mitchell, M. van Veenendaal, M. Daghofer, J. van den-Brink, G. Khaliullin, and B. J. Kim, Phys. Rev. Lett. **108**, 177003 (2012).
[13] J. Kim, M. Daghofer, A. H. Said, T. Gog, J. van den Brink, G. Khaliullin, and B. J. Kim, Nat. Commun. **5**, 4453 (2014).
[14] X. Liu, M. P. M. Dean, J. Liu, S. G. Chiuzbăian, N. Jaouen, A. Nicolaou, W. G. Yin, C. R. Serrao, R. Ramesh, H. Ding, and J. P. Hill, Journal of Physics: Condens. Matter **27**, 202202 (2015).
[15] X. Lu, P. Olalde-Velasco, Y. Huang, V. Bisogni, J. Pelliciari, S. Fatale, M. Dantz, J. G. Vale, E. C. Hunter, J. Chang, V. N. Strocov, R. S. Perry, M. Grioni, D. F. McMorrow, H. M. Ronnow, and T. Schmitt, Phys. Rev. B **97**, 041102 (2018).
[16] L. J. P. Ament, M. van Veenendaal, T. P. Devereaux, J. P. Hill, and J. van den Brink, Rev. Mod. Phys. **83**, 705 (2011).
[17] J. S. Lee, Y. Krockenberger, K. S. Takahashi, M. Kawasaki, and Y. Tokura, Phys. Rev. B **85**, 035101 (2012).
[18] J. P. Clancy, A. Lupascu, H. Gretarsson, Z. Islam, Y. F. Hu, D. Casa, C. S. Nelson, S. C. LaMarra, G. Cao, and Y.-J. Kim, Phys. Rev. B **89**, 054409 (2014).
[19] S. G. Chiuzbăian, C. F. Hague, A. Avila, R. Delaunay, N. Jaouen, M. Sacchi, F. Polack, M. Thomasset, B. Lagarde, A. Nicolaou, S. Brignolo, C. Baumier, J. Lüuning, and J.-M. Mariot, Review of Scientific Instruments **85**, 043108 (2014).
[20] M. Sacchi, N. Jaouen, H. Popescu, R. Gaudemer, J. M. Tonnerre, S. G. Chiuzbăian, C. F. Hague, A. Delmotte, J. M. Dubuisson, G. Cauchon, B. Lagarde, and F. Polack, Journal of Physics: Conference Series **425**, 072018 (2013).
[21] O. Bunau and Y. Joly, J. Phys. : Condens. Matter **21**, 345501 (2009).
[22] S. A. Guda, A. A. Guda, M. A. Soldatov, K. A. Lomachenko, A. L. Bugaev, C. Lamberti, W. Gawelda, C. Bressler, G. Smolentsev, A. V. Soldatov, Y. Joly, J. Chem. Theory Comput. **11**, 4512-4521 (2015).
[23] P. Blaha, K. Schwarz, G. Madsen, D. Kvasnicka, and J. Luitz, WIEN2K: An Augmented Plane Wave + Local Orbitals Program for Calculating Crystal Properties (Karlheinz Schwarz, Techniche Universitat, Wien, Austria)(1999).
[24] M. K. Crawford, M. A. Subramanian, R. L. Harlow, J. A. Fernandez-Baca, Z. R. Wang, and D. C. Johnston, Phys. Rev. B **49**, 9198 (1994).
[25] Peitao Liu, Bongjae Kim, Xing-Qiu Chen, D.D. Sarma, Georg Kresse, Cesare Franchini, Phys. Rev. Mater. 2, 075003 (2018)

[26] J. Jiménez-Mier, J. van Ek, D. L. Ederer, T. A. Callcott, J. J. Jia, J. Carlisle, L. Terminello, A. Asfaw, and R. C. Perera, Phys. Rev. B **59**, 2649 (1999).

[27] P. Glatzel, J. Singh, K. O. Kvashnina, and J. A. van Bokhoven, Journal of the American Chemical Society **132**, 2555 (2010).

[28] A. Louat, F. Bert, L. Serrier-Garcia, F. Bertran, P. Le Fevre, J. Rault, and V. Brouet, Phys. Rev. B **97**, 161109 (2018).

[29] C. H. Sohn, D.-Y. Cho, C.-T. Kuo, L. J. Sandilands, T. F. Qi, G. Cao, and T. W. Noh, Scientific Reports **6**, 23856 (2016).